Structures and adsorption energetics for chemisorbed fluorine atoms on Si(100)-2×1

Christine J. Wu and Emily A. Carter
Department of Chemistry and Biochemistry, University of California, Los Angeles, California 90024-1569
(Received 5 September 1991; revised manuscript received 2 December 1991)

We report first-principles electronic-structure calculations related to the initial fluorination of the Si(100)-2×1 surface. Embedded finite silicon clusters are used to model an extended Si(100)-2×1 surface. Two theoretical approaches, including a geometry-mapping procedure and an evaluation of lateral interactions via a dicluster model, are presented. Adsorption of up to 2.0 monolayers of fluorine is considered. Heats of adsorption, activation barriers, preferred binding sites, equilibrium geometries, charge transfer, and vibrational frequencies are predicted for this coverage range. Lateral interactions between various adspecies are found to be critically important in determining their stability. Thermochemical predictions derived from these calculations are used to postulate a reaction mechanism associated with the initial etching steps and with the adsorption kinetics of XeF_2 versus F_2.

I. INTRODUCTION

Chemical etching of silicon by a fluorine plasma is one of the most important materials tailoring techniques in the manufacture of semiconductor devices. A fluorine plasma produces a variety of high-energy, reactive atoms, ions, and even polyatomic radicals, which suggests that the etching mechanism is exceedingly complicated.[1–5] Although a great deal of experimental and theoretical effort has been expended,[1–30] the mechanism underlying the fluorine etching process is still not understood comprehensively. However, it is generally believed that atomic fluorine is the primary reactive agent in fluorine plasma etching.[1–3,5]

In the past ten years, the reactions of atomic F, F_2, and XeF_2 with Si(111), Si(100), and *a*-Si (amorphous silicon) have been studied intensively as simple models of the fluorine-silicon interactions involved in the actual plasma etching process.[6–21] Although F_2 and XeF_2 both chemisorb dissociatively to form $F_{(ad)}$, experiments have shown that reactions between atomic F, F_2, or XeF_2 and silicon each follow different kinetics.[7,8,11,12,19] X-ray photoelectron spectroscopy (XPS) studies of F and F_2 adsorption on Si(111) (Ref. 12) suggest that F_2 acts like low-pressure XeF_2, while F atoms behave more like high-pressure XeF_2. The kinetic differences between the precursors have been attributed primarily to the initial adsorption step, rather than the reaction or desorption steps.[10–12,19] In fact, steady-state exposures of XeF_2 or atomic F both lead to spontaneous etching at room temperature.[7,10]

It is commonly agreed upon that SiF_4 is the major etching product.[6,9,10,13] However, the relative abundances of reaction intermediates and other etch products (e.g., SiF_3, SiF_2, SiF, and polysilyl species) are still controversial. Winters and Houle demonstrated that the primary volatile product of the XeF_2 reaction with Si(111) is SiF_4 (~85%), with a small amount of SiF and SiF_2 radicals (~15%) also produced.[10] Si_2F_6 and SiF_3 were also observed as gas phase etch products.[13] However, Engstrom, Nelson, and Engel[18,19] found that exposure of Si(100) to an F_2 or mixed F and F_2 beam produces only SiF_2 at low coverages and a mixture of SiF_2 and SiF_4 at higher coverages. Steady-state etching of Si(111) produces an amorphous fluorosilyl layer about 10–20 Å thick, containing $SiF_{3(ad)}$ as the dominant adspecies, along with $SiF_{(ad)}$ and $SiF_{2(ad)}$ in smaller concentrations.[10,16,17] These observations suggest that formation of SiF_4 from SiF_3 may be the rate-limiting step.[10,16,17] However, earlier kinetic measurements using F atoms as the etchant found the activation energies for forming gas phase SiF_2 and SiF_4 to be almost the same, 0.092±0.02 and 0.15±0.02 eV,[9] consistent with reported values for the overall etching energy of 0.108±0.005 eV.[7] Therefore, formation of SiF_2 and SiF_4 are both possibly rate limiting. The etching activation energy is significantly higher (E_a = 0.4 eV) when F_2 is used as the reagent.[8] In sum, it appears that the product distribution (in both the gas phase and the adsorbed layer) and the initial reaction mechanism may be quite sensitive to the structure of the silicon surface [i.e., (111) versus (100)] and the fluorine reagent (i.e., F versus F_2 versus XeF_2).

Given the structure sensitivity discussed above, we limit our review of spectroscopic data to those for etching of Si(100), since this bears directly on the results presented herein. Shinn *et al.*[14] and McFeely *et al.*[15] examined the initial chemisorption of fluorine (via XeF_2) on the Si(100)-2×1 surface using low-energy electron diffraction (LEED), XPS, and electron-energy-loss spectroscopy (EELS). Shinn *et al.*[14] observed an SiF vibration at ~800 cm^{-1} in EELS, which they attributed to $SiF_{(ad)}$ and suggested that this was the primary adspecies at low coverage. The $p(2\times1)$ LEED pattern became more diffuse upon F adsorption, which indicated that the fluorosilyl layer was disordered. Since a 1×1 LEED pattern was not observed after saturation exposures, Shinn, Morar, and McFeely[14] concluded that the surface was not covered with SiF_2 groups. As presented below, our calculations rule out an adlayer of purely SiF_2 groups. Analysis of XPS spectra[15] taken at $\Theta_F \sim 2$ monolayers

 ©1992 The American Physical Society

(ML) revealed the major surface species to be $SiF_{(ad)}$ (1.16 ML) along with 0.39 ML of $SiF_{2(ad)}$ and a small amount of $SiF_{3(ad)}$ (0.11 ML).

Engstrom, Nelson, and Engel[18,19] measured the kinetics of adsorption for F_2 and F atoms on Si(100)-2×1 using modulated molecular beam (MMB) techniques, XPS, temperature-programmed desorption (TPD), and low-energy ion-scattering spectroscopy (LEISS). They observed a rapid rate of adsorption up to $\Theta_F = 1.5$ ML for F_2, followed by a much slower rate of fluorine incorporation. The initial adsorption probabilities for molecular and atomic fluorine are nearly identical (~ 0.5), but the F-atom adsorption probability decreases more slowly with coverage.

The only direct observations of the adsorbed fluorine surface geometry were recently reported by Bozack *et al.*[20] and Johnson, Walczak, and Madey,[21] who measured the electron-stimulated desorption ion angular distributions (ESDIAD) of adsorbed species on a partially fluorinated Si(100)-2×1 surface. The F^+ emission angle relative to the surface normal was found to be $36°\pm5°$ by Bozack *et al.* and $29°\pm3°$ by Johnson, Walczak, and Madey. Both groups suggest that this angle corresponds to the Si-F bond direction. In the work of Bozack *et al.*, the corresponding fluorine coverages and the surface compositions were not reported, making it difficult to interpret to which species the F^+ emission angle corresponds. The study by Johnson, Walczak, and Madey involved adsorption of HF onto Si(100), presumably forming a H-Si-Si-F monofluoro species.

Experimetal studies have contributed a great deal to our current understanding of the reactive species and pathways involved in chemical etching. However, little direct evidence for the primary steps involved in fluorine etching is available. Thus, it is useful to perform appropriate theoretical calculations able to examine many possible pathways, in order to evaluate various etching mechanisms.

Seel and Bagus reported a theoretical investigation of F on Si_xH_y ($x=4,10$; $y=9-15$) clusters as models for various sites on an unreconstructed Si(111) surface.[22] Since the clusters were rather large, only Hartree-Fock (HF) calculations were performed. The authors reported the binding energies for F on different sites and also barriers to penetrate into the subsurface layers. However, HF calculations do not provide reliable energetics. For example, the HF prediction for the first Si-F bond energy in SiF_4 is in error by about a factor of 2.[22] Later, Bagus reestimated the Si-F bond strength on an open threefold site to be ~ 4.0 eV, by correcting their previous HF value of ~ 0.5 eV with an estimated HF error of ~ 3.6 eV.[23] While these calculations are not quantitatively accurate, they did demonstrate that adsorption of F on silicon can be simulated appropriately using finite cluster models. Equilibrium properties at the HF level for F chemisorbed on Si_4H_9 and Si_9H_{15} cluster models of unreconstructed Si(111) were also predicted by Illas, Rubio, and Ricart[24] and Mohapatra *et al.*[25] Garrison and Goddard[26] proposed an S_N2 mechanism (bimolecular nucleophilic substitution) for the formation of SiF_4 from surface-bound SiF_3 groups, based on multiconfiguration–self-consistent-field calculations performed on $H_3Si\text{-}SiF_3+F$. In this S_N2 process, an F atom attacks the backside of the SiF_3 group to form SiF_4, which would then desorb. Finally, local-density-approximation (LDA) cluster[27] and slab[28,29] calculations of F-atom adsorption and absorption on Si(111) have also been carried out.

All of the above calculations examined etching of the unreconstructed Si(111) surface rather than the technologically more important Si(100) surface. Recently, Craig and Smith[30] reported the only related study on the Si(100)-2×1 surface for adsorption of a monolayer of HF or F_2 using a semiempirical method. F atoms were found to form stable bonds to the 2×1-reconstructed Si surface. Geometries for F adsorbed on the surface Si dimers were calculated as well.

Since experiments have demonstrated that the initial etching steps are surface structure dependent, it is useful to carry out first-principles calculations (including electron correlation) on larger cluster models that better characterize the actual surface structure. Given the lack of direct experimental data probing elementary reaction steps and the lack of high level calculations for fluorine adsorption on Si(100), we have undertaken a study of the initial stages of fluorinating the Si(100)-2×1 reconstructed surface. We carried out first-principles electronic-structure calculations of atomic F bound to embedded finite silicon clusters (*vide infra*) to serve as models for the localized bonding interactions present on an extended Si(100)-2×1 surface. These calculations include the dominant electron correlation effects [at the generalized valence bond[31] (GVB) level, along with correlation-consistent configuration interaction[32,33] (CCCI)] required to obtain accurate energetics (errors of $\sim 0.1-0.2$ eV). In this paper, we predict heats of reaction, activation barriers, and equilibrium surface configurations as a function of fluorine coverage up to 2.0 ML. In addition, we report the local equilibrium geometries, the extent of charge transfer, bond character, and harmonic vibrational frequencies for surface fluorosilyl species. We then compare our results with related previous experimental and theoretical data. Based on our calculations, we propose a reaction mechanism for the beginning stages of the etching process.[34]

II. CALCULATIONAL DETAILS

A. Surface reaction models

The Si(100)-2×1 surface reconstruction produces a unit cell that contains a Si-Si σ bond and two singlet-coupled dangling bonds between two neighboring surface Si atoms forming a so-called Si dimer.[35]

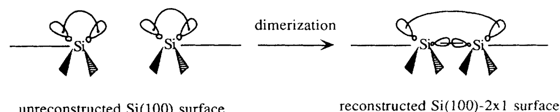

We model the Si(100)-2×1 surface by finite silicon clusters in which the subsurface silicon atoms are constrained to bond tetrahedrally to the atoms around them (as in the crystal) by saturating the subsurface dangling bonds with

hydrogen atoms. However, in order to avoid unrealistic charge transfer that would occur between silicon and hydrogen, modified hydrogen atoms ($\overline{H}$), with basis sets adjusted to have the same electronegativity as silicon, were used to embed the subsurface atoms in the clusters (see Sec. II B).

The larger clusters employed in our calculations, such as $Si_9\overline{H}_{12}$ [shown in Fig. 1(a)], consist of nine Si atoms (two surface Si atoms representing a surface Si dimer, four second-layer Si atoms, two third-layer Si atoms, and one fourth-layer Si atom) and are embedded in 12 $\overline{H}$ atoms. In order to carry our large configuration-interaction (CI) calculations, we developed a strategy of geometry mapping (GM), which appears to be accurate to $\sim$0.1 eV.[36] It works as follows. We employ large clusters to obtain fully gradient-optimized (*vide infra*) geometries at the GVB level of theory. Then we utilize those geometries to fix atomic positions in smaller clusters that are used in CI calculations to obtain bond energies and heats of reaction. The GM procedure is shown in Fig. 1, where (a) is mapped onto (b), (c) onto (d), and (e) onto (f). Based on the largest CI calculations we can carry out on both the large and small clusters (a complete active space CI, i.e., a full CI within the GVB orbitals), we estimate the error incurred by using the smaller clusters to represent the surface to be $\sim$0.1 eV (*vide infra*).

The above calculations indicate that the dominant physics in chemisorption on covalently bonded materials such as silicon is captured by properly describing the *local* surface wave function. To take a specific example, the predicted reconstructed Si(100)-2$\times$1 surface geometry is derived from optimization of the unreconstructed cluster $Si_9\overline{H}_{12}$. Since $Si_9\overline{H}_{12}$ is too large a cluster on which to perform high level CI calculations, we mapped the geometry obtained from $Si_9\overline{H}_{12}$ onto a cluster where all subsurface atoms are replaced with $\overline{H}$, i.e., a $Si_2\overline{H}_4$ cluster with the Si-$\overline{H}$ bond length R(Si-$\overline{H}$) fixed at 1.729 Å [taken from R(Si-$\overline{H}$) of the optimized larger clusters]. Then CI calculations are carried out on this small GM cluster.

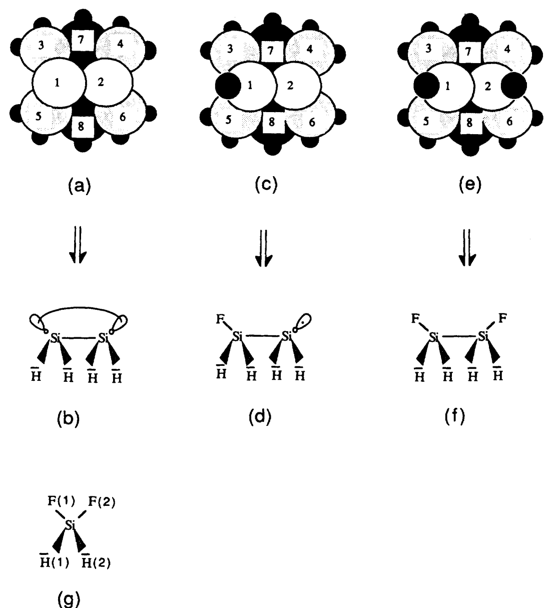

FIG. 1. Schematic pictures of silicon clusters used in calculations for modeling (i) the bare Si(100)-2$\times$1 surface by (a) the fully optimized $Si_9\overline{H}_{12}$ cluster and (b) the GM-$Si_2\overline{H}_4$ cluster; (ii) a half-fluorinated silicon dimer (Si-Si-F) by (c) the fully optimized $Si_9\overline{H}_{12}F$ cluster and (d) the GM-$Si_2\overline{H}_4F$ cluster; (iii) a fully fluorinated silicon dimer (F-Si-Si-F) by (e) the fully optimized $Si_9\overline{H}_{12}F_2$ cluster and (f) the GM-$Si_2\overline{H}_4F_2$ cluster; and (iv) a difluorosilyl species (SiF_2) by (g) the fully optimized $Si_2\overline{H}_2F_2$ cluster. Si atoms in the $Si_9\overline{H}_{12}$ clusters are numbered from the surface layer downward. Small black circles represent $\overline{H}$ atoms. The fourth-layer Si atom is not shown. Medium-sized gray circles represent F atoms.

Qualitative evidence for the success of this geometry mapping idea is illustrated in Fig. 2, where we compare the surface wave functions of the silicon dimer (two dangling-bond orbitals and the silicon σ bond) in the optimized $Si_9\overline{H}_{12}$ cluster with those of the GM-$Si_2\overline{H}_4$ and the relaxed $Si_2\overline{H}_4$ clusters. The relaxed $Si_2\overline{H}_4$ cluster has two dangling-bond orbitals almost normal to the "surface" that form a π bond, while the dangling-bond orbitals in the GM-$Si_2\overline{H}_4$ cluster look essentially identical to those of the larger $Si_9\overline{H}_{12}$ cluster. The Si-Si bonds in all three clusters are similar, although the Si-Si bond in the relaxed $Si_2\overline{H}_4$ cluster has less p character (63%) than in the more realistic $Si_9\overline{H}_{12}$ or the GM-$Si_2\overline{H}_4$ clusters (76% and 82%, respectively) due to the formation of a Si-Si π bond that is purely p in character in the relaxed $Si_2\overline{H}_4$ cluster. Thus, the relaxed $Si_2\overline{H}_4$ cluster in no way represents the surface properly: geometry mapping is critical to obtaining the proper local wave function.

B. Basis sets

Since the Si clusters we studied were quite large, all of the core electrons of the Si atoms were replaced by effective core potentials, ECP's, while all Si valence electrons were treated explicitly with double-ζ (DZ) contracted Gaussian basis sets.[37] Additional d polarization functions (ζ^d=0.3247) were added to the surface Si atoms. A triple-ζ basis set contracted to a minimal basis (i.e., where the coefficient ratios are fixed between the three functions) was optimized for the $\overline{H}$ atoms using a $Si(Si\overline{H}_3)_4$ cluster. The criterion for optimization was that the central Si atom be neutral, following the idea of Redondo *et al.*[38] The resulting $(3s/1s)$ minimum basis set for the $\overline{H}$ atoms is listed in Table I. The radial extent of this orbital is very similar to a Si 3s orbital. For F atoms, we used the Dunning $(9s5p/3s2p)$ valence DZ contraction[39] of the Huzinaga primitive Gaussian basis set,[40] one set of d polarization functions (ζ^d=1.34), and one set of diffuse s and p functions (ζ^s=0.112 and ζ^p=0.076). We denote this F basis as VDZP + DIF.

C. GVB calculations, geometry optimizations, and vibrational frequencies

In all of the GVB calculations, the important bond pairs were described at the GVB perfect pairing (GVB-PP) level,[31] while all other electron pairs were treated at the HF level. Thus, for the $Si_9\overline{H}_{12}(^1A_1)$ cluster, the σ bond and the singlet-coupled dangling bonds of the Si di-

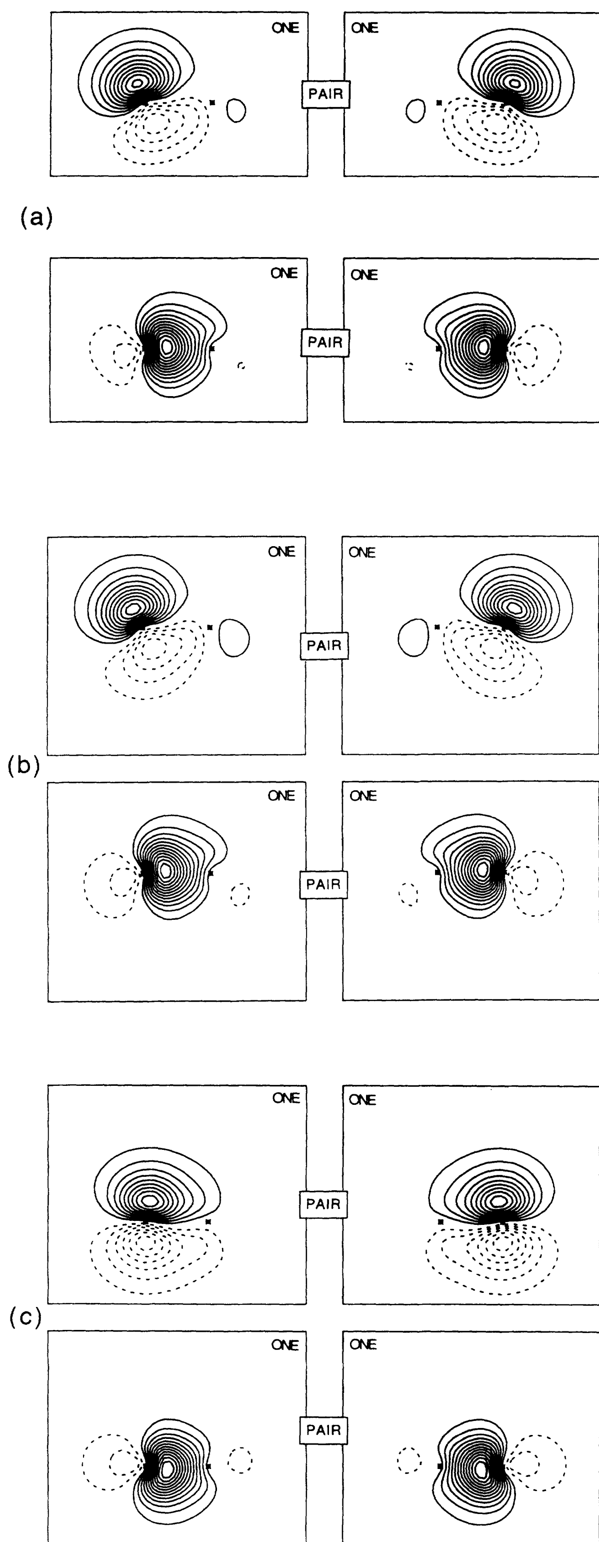

FIG. 2. Contour plots of one-electron GVB orbitals for the silicon dangling-bond pair (top) and the silicon dimer σ-bond pair (bottom) for (a) the optimized $Si_9\overline{H}_{12}(^1A_1)$; (b) the GM-$Si_2\overline{H}_4(^1A_1)$; and (c) the optimized $Si_2\overline{H}_4(^1A_1)$ clusters. Spacing between the contours is 0.02 a.u. Solid lines represent positive amplitude, while dashed lines represent negative amplitude. The same convention is used in all plots.

TABLE I. Gaussian $(3s/1s)$ minimum basis set for the $\overline{H}$ atom (see text).

i	ζ_i	C_i
1	1.150476	0.558913
2	0.270400	−1.304640
3	0.132320	2.80000

mer were correlated as GVB pairs. For fluorinated clusters, we always treated the Si-F bonds as additional GVB pairs. GVB($N/2N$) calculations were carried out, where N equals the number of correlated electron pairs and $2N$ equals the number of natural orbitals (two per GVB pair).[31] The geometries of the bare and fluorinated large clusters ($Si_9\overline{H}_{12}$, $Si_9\overline{H}_{12}F$, and $Si_9\overline{H}_{12}F_2$) were optimized self-consistently at the GVB-PP level by analytic gradient techniques.[41,42] At the same time, harmonic vibrational frequencies were calculated via diagonalization of numerical mass-weighted second derivative matrices.[41,42]

D. CI calculations

Generalized valence bond theory with the correlation-consistent configuration-interaction method was used to obtain our final predictions of energetics. This method has been shown to provide predictions of known single bond dissociation energies to within 0.1–0.2 eV.[32,43,44] The first-order GVB wave functions were utilized as a basis for the CCCI calculations. From the RCI (restricted CI, which allows direct products of all three possible configurations in each GVB pair; i.e., 3^N configurations for N GVB pairs) reference space, the CCCI technique allows all single and double excitations from the active electron pair(s) involved in the process of interest ($RCI^*[SD_{pair\,1}+SD_{pair\,2}+\cdots]$). Additionally, all single excitations from all valence orbitals are included (S_{val}), to account for orbital hybridization changes during a reaction. This method is nearly size-consistent (to within $\sim$0.01 eV) (Ref. 32) and includes most of the important electron correlation, leading to quite accurate predictions of bond energies. Upon dissociation, the corresponding fragments are treated at the same level, where now SD becomes S_{val} because the bond has disappeared. For the F atom, this means HF^*S_{val}, which turns out to have the same total energy as the HF total energy (to the microhartree level).

Complete active space CI calculations, defined here as a full CI within the GVB space (GVB-CI), were also carried out. Multiconfiguration–self-consistent-field (MCSCF) calculations were performed for processes involving multiple resonance structures, where the GVB-PP wave function would have restricted the description to only one resonance structure. The MCSCF wave functions were also employed in resonance-CCCI calculations, which included the relevant resonance structures in the reference space. We find that the differential changes in zero-point energies are very small ($\sim$0.05–0.09 eV) between different fluorinated clusters, and hence the reported bond energies, D_e, are essentially the same as D_0 (within our error bars).

E. Evaluation of lateral interactions

Lateral interactions between fluorosilyl groups were calculated at the GVB-PP level by varying the distance between two rigidly oriented clusters. Counterpoise corrections for basis-set superposition errors[45] were included in the evaluation of these nonbonded interactions, at each distance that the lateral repulsions were evaluated. The resulting interaction energies then were added to the heats of adsorption and/or reaction calculated for the zero coverage limit, in order to estimate heats of reaction and/or adsorption at specific coverages. Furthermore, a criterion of minimum repulsion was used to extract equilibrium positions for the adspecies at various coverages. Examples follow in Sec. III.

III. RESULTS AND DISCUSSION

We investigated a number of possible pathways at different fluorine coverages (Θ_F): $\Theta_F \le 0.5$ ML; 0.5 ML $< \Theta_F \le 1.0$ ML; 1.0 ML $< \Theta_F \le 1.5$ ML; and 1.5 ML $< \Theta_F \le 2.0$ ML, where 1 ML is defined by the number of surface atoms on Si(100).

A. Addition of F atoms to the clean Si(100)-2×1 surface ($\Theta_F \le 0.5$ ML)

Two high-symmetry pathways and subsequent adsorption sites were examined: (i) adsorption of an F atom directly onto a Si dangling bond to form a monocoordinated F atom, and (ii) adsorption of an F atom directly on top of a Si dimer to form a bridging, dicoordinated F atom. Redondo and Goddard[46] previously predicted that the coupling between the Si dangling bonds on a Si dimer is very weak, with a singlet-triplet splitting of $\Delta E_{ST} \sim 0.03$ eV. We have confirmed this with our fully optimized structure of $Si_9\overline{H}_{12}$, where we find $\Delta E_{ST} = 0.025$ eV. Therefore, those dangling bonds on the surface atoms are quite similar in nature to radical electrons and hence should be highly reactive. Given the direction of the dangling bonds outward from the Si dimer bond [see Fig. 1(b)], one might expect that monocoordinated Si-F bond formation is more likely to occur. Indeed, our calculations indicate that if an F atom approaches a dangling bond of a Si dimer, it forms an extremely strong Si-F bond worth 6.4 eV, with no activation barrier associated with this bond formation. We also find that an F atom can form a stable bridge bond (worth 3.0 eV) with a Si dimer. However, in the latter case we find that no barrier exists for the bridging F atom to slide toward a silicon dimer dangling bond to form the more stable monocoordinated Si-F bond. We now consider in turn both cases in more detail.

1. F adsorption onto the dangling bond of a Si dimer

Figure 1(c) depicts the optimized structure of the $Si_9\overline{H}_{12}F$ cluster, where the F atom is bound to a dimer dangling bond. Table II shows the predicted geometrical parameters, with a predicted equilibrium Si-F bond length $R(\text{Si-F}) = 1.646$ Å, a Si dimer bond length $R(\text{Si}_d\text{-Si}_d) = 2.426$ Å, and a surface Si-atom–second-layer Si-atom bond length $R(\text{Si}_d\text{-Si}_{sub}) = 2.350$ Å. The latter value for $R(\text{Si}_d\text{-Si}_{sub})$ is in exact accord with the known bulk bond length in Si,[47] while the Si-Si dimer bond length (which lengthens by only 0.18 Å from the bare dimer upon fluorination) is in good agreement with experimental values for the Si dimer bond length (2.36–2.47 Å).[35] The Si-Si bond lengths remain nearly constant before and after addition of atomic F, in accordance with the localized bonding picture and the weak coupling between the dimer dangling bonds. Our prediction of a Si-F bond length of 1.646 Å is consistent with typical Si-F bond lengths of ~1.6 Å for gas phase molecules [e.g., $R(\text{Si-F}) = 1.590$ and 1.598 Å for SiH_3F and Si_2H_5F, respectively].[48] Since no surface Si-F bond lengths have been elucidated experimentally, the only other comparison we can make is with the semiempirical calculations

TABLE II. The important internal coordinates of the optimized $Si_9\overline{H}_{12}F$ cluster. Labels refer to Fig. 1(c).

Bond length (Å)		Bond angle (deg)	
R(F-Si(1))	1.646	θ(F-Si(1)-Si(2))	113.4
R(Si(1)-Si(2))	2.426	θ(F-Si(1)-Si(3)) $=\theta$(F-Si(1)-Si(5))	114.0
R(Si(1)-Si(3)) $=R$(Si(1)-Si(5))	2.350	θ(Si(3)-Si(1)-Si(2)) $=\theta$(Si(5)-Si(1)-Si(2))	105.3
R(Si(2)-Si(4)) $=R$(Si(2)-Si(6))	2.360	θ(Si(4)-Si(2)-Si(1)) $=\theta$(Si(6)-Si(2)-Si(1))	104.1
R(Si(3)-Si(7)) $=R$(Si(5)-Si(8))	2.361	θ(Si(3)-Si(1)-Si(5))	103.8
		θ(Si(4)-Si(2)-Si(6))	101.7
R(Si(4)-Si(7)) $=R$(Si(6)-Si(8))	2.365		
R(Si(7)-Si(9)) $=R$(Si(8)-Si(9))	2.352		
R(Si(3)-Si(4)) $=R$(Si(5)-Si(6))	3.624		
R(Si(3)-Si(5))	3.698		
R(Si(4)-Si(6))	3.660		

for HF adsorbed on Si(100).[30] Their values of R(Si-F)=1.760 Å and $R(\mathrm{Si}_d\text{-}\mathrm{Si}_d)$=2.406 Å are close to our predictions. The angle between a Si-F bond and the Si dimer is predicted to be 113.4° or 23.4° away from the surface normal. This is in reasonable agreement with ESDIAD data of a 29°±3° or 36°±5° tilt of F away from the surface normal on Si(100)-2×1,[20,21] especially considering that image charge effects may act to increase the measured bond angle (equated with the F^+ trajectory direction). The predicted Si-Si-F angle is also in accord with the semiempirical prediction of 110.1°.

The harmonic vibrational frequencies of the optimized $Si_9\bar{H}_{12}F$ cluster were obtained from a normal mode analysis, which gives rise to a fairly localized stretching mode of the Si-F bond at 924 cm^{-1}. Other F-derived modes (e.g., bending frequencies) coupled with motions of substrate silicon atoms occur at ~158–376 cm^{-1} (in the range of the silicon bulk phonon frequencies). Shinn, Morar, and McFeely[14] observed a Si-F derived loss in EELS at ~800 cm^{-1}, in the same spectral region as our prediction.

In order to understand doping effects on etching, it is important to discern the extent to which F resembles an ion or a neutral atom on the Si(100)-2×1 surface. We calculated the charge distributions for the F, Si, and $\bar{H}$ atoms in the optimized $Si_9\bar{H}_{12}F$ cluster by Mulliken population analysis (listed in Table III). Although this technique is basis set dependent, it yields a generally reliable qualitative picture. We find that 0.38e is transferred to the adsorbed fluorine primarily from the silicon atom that forms the Si-F bond. The other silicon atom on the surface dimer and all subsurface silicon atoms remains nearly neutral, i.e., with about the same charge distribution as in the bare $Si_9\bar{H}_{12}$ cluster. The embedded $\bar{H}$ atoms also remain virtually neutral. Thus, the adsorption of F onto the dangling bond of a Si dimer leads to a Si-F bond with localized ionic character.

As explained in Sec. II, the GM-$Si_2\bar{H}_4$ and $Si_2\bar{H}_4F$ clusters were constructed from the geometries of the optimized $Si_9\bar{H}_{12}$ and $Si_9\bar{H}_{12}F$ clusters. These smaller GM clusters are depicted schematically in Figs. 1(b) and 1(d). Contour plots of the one-electron GVB orbitals of the remaining dangling orbital of the Si dimer, the Si-F σ bond pair, and the Si-Si dimer σ bond pair for the optimized $Si_9\bar{H}_{12}F$ and the GM-$Si_2\bar{H}_4F$ clusters are plotted in Figs. 3(a) and 3(b), respectively. As in the case of the bare clusters, the surface wave function represented by the optimized $Si_9\bar{H}_{12}F$ cluster is extremely similar to that of the GM-$Si_2\bar{H}_4F$ cluster. In addition, the contour plot of the Si-F bond pair demonstrates unequivocally that the Si-F bond is localized at the surface. Thus, the Si-F bond of the GM-$Si_2\bar{H}_4F$ cluster should adequately represent the Si-F interaction on the Si(100)-2×1 surface.

As in our previous calculations of bond dissociation energies,[32,43,44] we constructed a thermodynamic cycle to obtain correlation-consistent energetics (see Fig. 4). Since the fluorinated dimer has silicon orbitals that most closely resemble uncoupled Si dangling bonds, we break the Si-F bond to form the $^3B_1$ state of the dimer, which is then allowed to relax to its $^1A_1$ ground state. The first Si-F bond strength calculated from both the larger clusters ($Si_9\bar{H}_{12}$ and $Si_9\bar{H}_{12}F$) and the smaller GM clusters ($Si_2\bar{H}_4$ and $Si_2\bar{H}_4F$) is listed as a function of increasing electron correlation in Tables IV and V, respectively. The GVB-CI calculations on the larger and the smaller GM clusters predict Si-F bond strengths of 4.7 and 4.8 eV, respectively. Thus, as mentioned in Sec. II, errors introduced by using the smaller model clusters with the same geometry as the larger cluster are ~0.1 eV at comparable levels of electron correlation. In order to illus-

TABLE III. The net charges (a.u.) for F, Si, and $\bar{H}$ atoms obtained from Mulliken population analyses for optimized and geometry-mapped bare and fluorinated silicon clusters.

Positions	Centers	$Si_9\bar{H}_{12}$	$Si_9\bar{H}_{12}F$	$Si_9\bar{H}_{12}F_2$	GM-$Si_2\bar{H}_4$	GM-$Si_2\bar{H}_4F$	GM-$Si_2\bar{H}_4F_2$	$Si\bar{H}_2F$	$Si\bar{H}_2F_2$
Adsorbate	F		−0.38	−0.39		−0.21	−0.22	−0.16	−0.21
Surface layer	Si	+0.04	+0.42[a] +0.08[b]	+0.44	−0.06	+0.17[a] −0.06[b]	+0.16	+0.14	+0.41
Second layer	Si	−0.12	−0.15[c] −0.13[d]	−0.15					
	$\bar{H}$[e]	+0.05 +0.04	+0.06 +0.05 +0.04 +0.03	−0.07 −0.05	+0.03	+0.03[c] +0.02[d]	+0.03	+0.01	+0.01
Third layer	Si	−0.01	−0.05	−0.06					
	$\bar{H}$[e]	+0.06	+0.08	+0.09					
Fourth layer	Si	−0.15	−0.14	−0.14					
	$\bar{H}$[e]	+0.06	+0.06	+0.06					

[a]Net charge for the Si atom bonded to the F atom.
[b]Net charge for the Si atom with a dangling orbital.
[c]Net charge for an atom bonded to the surface Si described in footnote a.
[d]Net charge for an atom bonded to the surface Si described in footnote b.
[e]$\bar{H}$ atoms listed in each layer are the ones that are attached to the Si atoms in that layer.

trate the importance of this theoretical strategy, we also carried out calculations of the Si-F bond energy using $Si_2\overline{H}_4F$ and $Si_2\overline{H}_4$ clusters with relaxed geometries (i.e., optimized for the small cluster itself). The Si-F bond energies and adiabatic singlet-triplet splittings for the latter calculations are listed in Tables V and VI, respectively. Most of the energetic difference between fluorinating the relaxed $Si_2\overline{H}_4$ cluster and the GM-$Si_2\overline{H}_4$ cluster is due to the singlet-triplet splitting of $Si_2\overline{H}_4$. As shown in Fig. 2(c), the optimized structure of $Si_2\overline{H}_4$ converts the dangling-bond pair into a π bond, which results in a singlet-(*cis*) triplet splitting that is much higher ($\Delta E_{ST}=1.0$ eV) than those of the GM-$Si_2\overline{H}_4$ ($\Delta E_{ST}\cong 0.2$ eV) and optimized $Si_9\overline{H}_{12}$ ($\Delta E_{ST}=0.03$ eV) clusters.

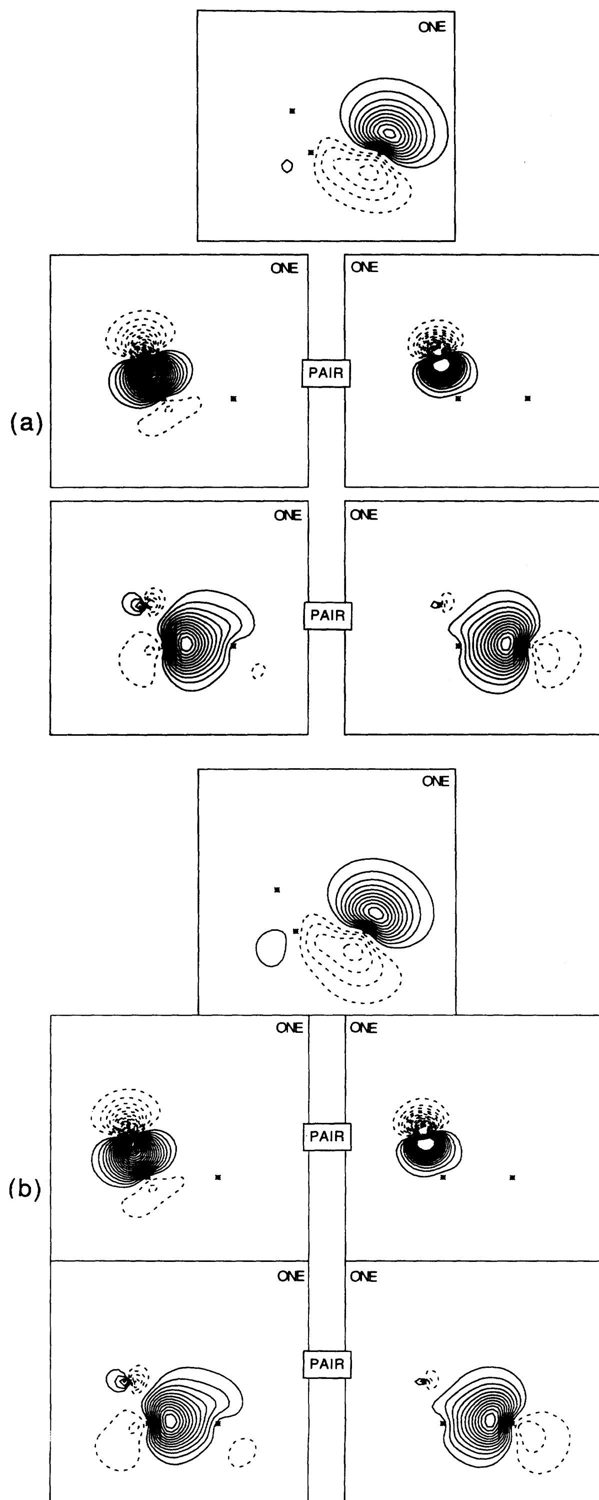

FIG. 3. Contour plots of one-electron GVB orbitals for the remaining silicon dangling orbital (top), Si-F σ-bond pair (middle), and the silicon dimer σ-bond pair (bottom) for (a) the optimized $Si_9\overline{H}_{12}F(^2A')$ and (b) the GM-$Si_2\overline{H}_4F(^2A')$ clusters.

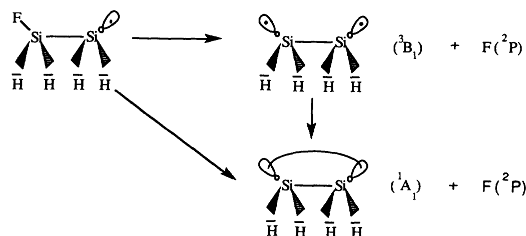

FIG. 4. The thermodynamic cycle for calculating the Si-F bond strength of a Si-Si-F species.

The CCCI calculations for the GM $Si_2\overline{H}_4$ and $Si_2\overline{H}_4F$ clusters predict that fluorine forms an extremely strong bond of 6.4 eV to a dangling bond of a silicon dimer. Experimental Si-F surface thermochemistry is not available for direct comparison. However, we can compare to the experimental gas phase SiH_3-F bond strength of 6.7 ± 0.4 eV,[49,50] which is close to our prediction.

We also calculated a trajectory for F attacking Si(100)-2×1 along the dimer dangling-bond direction [Θ(F-Si-Si)$=113.4°$] on the rigid GM-$Si_2\overline{H}_4$ cluster.

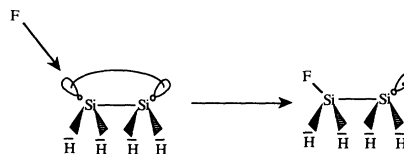

The potential curves calculated at the GVB-CI and CCCI levels are plotted in Fig. 5. This reaction experiences no activation barrier, suggesting that the initial sticking probability of atomic F may be close to unity. This is consistent with empirical[51] and *ab initio* derived[52] dynamical simulations that found a near unity sticking probability. By contrast, Engstrom, Nelson, and Engel[19] report $S_0=0.5\pm0.3$ for a mixed F_2 and F beam scattering off of Si(100). The discrepancy between theory and experiment may be due to perturbations caused by the presence of F_2 or due to the inherent limitations on detection via XPS (0.1–0.2 ML).

2. F atom adsorption in a bridge site on a Si dimer

We also studied chemisorption of atomic F at a twofold site of the Si(100)-2×1 surface, forming a dimer bridge bond with the two resonance structures shown below.

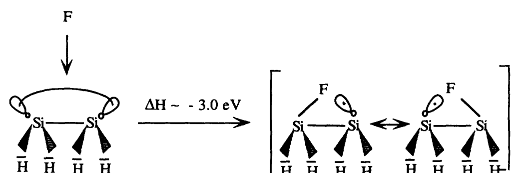

TABLE IV. The first and second Si-F bond dissociation energies (D_e, in eV) of an F-Si-Si-F species obtained from the optimized $Si_9\overline{H}_{12}$-F and $Si_9\overline{H}_{12}$F-F cluster calculations. The HF total energy for the F atom within the VDZP + DIF basis used here is −99.395 61 hartrees. 1 hartree is equal to 627.5096 kcal/mol = 27.211 62 eV = 219 474.8 cm^{-1}. Equilibrium geometries optimized at the GVB-PP level are used for all molecules (see text).

Calculation[a]	$Si_9\overline{H}_{12}$ ($^3B_1$)	$Si_9\overline{H}_{12}F$ ($^2A'$)	$Si_9\overline{H}_{12}F_2$ ($^1A_1$)	$D_e(Si_9\overline{H}_{12}$-F)[b]	$D_e(Si_9\overline{H}_{12}$F-F)[c]
	Total energies (hartrees)				
HF	−2605.213 98 (1/1)	−2704.766 18 (1/1)	−2804.317 62 (1/1)	4.2	4.2
GVB-PP	−2605.221 23 (2/2)	−2704.791 80 (4/4)	−2804.317 62 (8/8)	4.7	4.7
GVB-RCI	−2605.221 26 (4/4)	−2704.791 92 (9/17)	−2804.361 77 (27/37)	4.7	4.7
GVB-CI	−2605.223 29 (8/8)	−2704.793 36 (51/75)	−2804.362 709 (141/175)	4.7	4.7

[a]The corresponding number of spatial configurations and spin eigenfunctions for each wave function are given beneath each total energy. The orbitals are optimized self-consistently at the GVB-PP level.
[b]$D_e(Si_9\overline{H}_{12}\text{-F}) = E(Si_9\overline{H}_{12}, {}^3B_1) + E(F, {}^2P) - E(Si_9\overline{H}_{12}F, {}^2A') - \Delta E_{ST}$, where ΔE_{ST} is the singlet-triplet splitting of the $Si_9\overline{H}_{12}$ cluster ($\Delta E_{ST} = 0.03$ eV) at the RCI*$SD_{\text{dangling bond}}$ level ($^1A_1$ total energy is equal to −2605.243 59 hartrees and $^3B_1$ total energy is equal to −2605.242 67 hartrees).
[c]$D_e(Si_9\overline{H}_{12}F\text{-F}) = E(Si_9\overline{H}_{12}F, {}^2A') + E(F, {}^2P) - E(Si_9\overline{H}_{12}F_2, {}^1A_1)$.

The GM-$Si_2\overline{H}_4$ cluster was used to mimic a rigid surface dimer. Surface relaxation during bridge bond formation was not considered, therefore the binding energy we calculate is a lower bound to the exact binding energy. The potential curves calculated at the generalized valence bond–configuration interaction–self-consistent field (GVB-CI-SCF) and CCCI levels are plotted in Fig. 6 for approach of F along the surface normal direction at the midpoint of the Si-Si dimer bond. The resonance structures make it important to correlate the Si-Si σ and the dangling bonds of the dimer, as well as the three F $2p$ electrons that reside in the bonding plane. Those seven electrons are treated via a full CI within six orbitals in the GVB-CI calculations. The GVB-CI-SCF calculations then allow the orbital shapes to change from the GVB-PP orbitals to orbitals optimized for the GVB-CI. The GVB-CI-SCF results suggest that atomic F can form a stable twofold bridge bond to the dimer, with an equilibrium perpendicular distance from the surface ($R_{\perp,\text{eq}}$) of 1.6 Å. The barrier associated with this pathway is almost negligible ($E_a \sim 0.03$ eV). Higher-order CCCI calculations were performed in order to estimate the bond energy more accurately. The CCCI calculations began with the GVB-CI-SCF wave functions as the first-order wave function and included both resonance configurations in the multireference space. Resonance-CCCI predicts a bridging Si-F-Si bond strength of 3.0 eV, much weaker than the heat of adsorption of 6.4 eV for monocoordinat-

TABLE V. The Si-F bond energy of an F-Si-Si species (D_e, in eV) obtained from calculations of the optimized $Si_2\overline{H}_4F$ and $Si_2\overline{H}_4$ clusters, and the GM-$Si_2\overline{H}_4$ and the GM-$Si_2\overline{H}_4$F clusters.

Calculation[a]	$Si_2\overline{H}_4F$ ($^2A'$)	$Si_2\overline{H}_4$ ($^3B_1$)	D_e ($Si_2\overline{H}_4$-F)[b]	GM-$Si_2\overline{H}_4F$ ($^2A'$)	GM-$Si_2\overline{H}_4$ ($^3B_1$)	D_e (GM-$Si_2\overline{H}_4$-F)[c]
	Geometry optimized cluster			Geometry-mapped (GM) cluster		
	Total energies (hartrees)			Total energies (hartrees)		
GVB(2/4)-PP	−679.171 42 (4/4)	−579.590 08 (2/2)	4.1	−679.112 80 (4/4)	−579.537 86 (2/2)	4.9
GVB-RCI(2/4)	−679.171 90 (9/17)	−579.590 19 (4/4)	4.1	−679.112 89 (9/17)	−579.537 94 (4/4)	4.9
GVB-CI(2/4)	−679.172 11 (19/35)	−579.591 94 (8/8)	4.0	−679.113 43 (19/35)	−579.540 30 (8/8)	4.8
GVB-RCI(2/4)*$SD_{\text{Si-F}}$	−679.179 03 (1337/3645)	−579.594 80 (34/62)	4.1	−679.120 00 (1337/3645)	−579.542 44 (34/62)	4.9
CCCI(2/4)	−679.242 57 (2940/10 070)	−579.604 41 (192/432)	5.6	−679.184 71 (2940/10 070)	−579.552 78 (192/432)	6.4

[a]The corresponding number of spatial configurations and spin eigenfunctions for each wave function are given beneath each total energy. The geometries of $Si_2\overline{H}_4$ and $Si_2\overline{H}_4F$ clusters were optimized at the GVB(2/4)-PP level, while the geometries of the GM-$Si_2\overline{H}_4$ and GM-$Si_2\overline{H}_4F$ clusters were taken from the optimized $Si_9\overline{H}_{12}$ and $Si_9\overline{H}_{12}F$ clusters (see text).
[b]$D_e(Si_2\overline{H}_4\text{-F}) = E(Si_2\overline{H}_4, {}^3B_1) + E(F, {}^2P) - E(Si_2\overline{H}_4F, {}^2A') - \Delta E_{ST}$, where $\Delta E_{ST} = 1.0$ eV, taken from the singlet-triplet splitting of the optimized $Si_2\overline{H}_4$ cluster (see Table VI).
[c]$D_e(\text{GM-}Si_2\overline{H}_4\text{-F}) = E(\text{GM-}Si_2\overline{H}_4, {}^3B_1) + E(F, {}^2P) - E(\text{GM-}Si_2\overline{H}_4F, {}^2A') - \Delta E_{ST}$, where $\Delta E_{ST} = 0.03$ eV, taken from the singlet-triplet splitting of the optimized $Si_9\overline{H}_{12}$ cluster.

TABLE VI. Singlet-triplet splittings (ΔE_{ST}) and total energies for $^1A_1$ and $^3B_1$ states of the optimized $Si_2\overline{H}_4$ cluster.

Calculation[a]	Total energies (hartrees) $^1A_1$	$^3B_1$	ΔE_{ST} (eV)
GVB(2/4)-PP	−579.616 38 (4/4)	−579.590 08 (2/2)	0.7
GVB-RCI(2/4)	−579.624 30 (9/10)	−579.590 19 (4/4)	0.9
GVB-CI(2/4)	−579.623 68 (19/20)	−579.591 94 (8/8)	0.9
GVB-RCI(2/4)*$(SD)_{DB}$[b]	−579.632 31 (549/697)	−579.595 67 (268/404)	1.0

[a]The corresponding number of spatial configurations and spin eigenfunctions for each wave function are given beneath each total energy. The orbitals are optimized self consistently at the GVB(2/4)-PP level.

[b]DB denotes dangling bonds.

ed fluorine. Thus, a thermodynamic preference exists for the first F atom to attack the dangling bond rather than the Si-Si bond of a dimer.

Given the greater stability of monocoordinated over bridging F atoms, it is likely that F atoms adsorbed initially near a bridge site will convert to onefold $F_{(ad)}$. We investigated this diffusion of F from the bridge to the dangling-bond site by generating potential curves for an F atom moving from the equilibrium bridge bond position ($R_{\parallel}=0$ Å) toward a dangling bond of the silicon dimer, keeping the vertical distance fixed between the F atom and the Si(100)-2×1 surface at $R_{\perp,eq}=1.6$ Å.

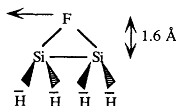

Substrate relaxation was not allowed. The resulting potential curves at the GVB-CI and CCCI levels are shown in Fig. 7, where we see that no activation barrier is associated with this motion. The minimum position in the potential curve ($R_{\parallel}=1.6$ Å, $R_{\perp}=1.6$ Å) is exactly at the equilibrium position of the Si-F bond in the fully optimized $Si_9\overline{H}_{12}F$ cluster [R_e(Si-F)=1.646 Å], lending credence to the rigid cluster approximation used in this last set of calculations.

In summary, we find that at low coverages of fluorine on Si(100)-2×1 ($\Theta_F \le 0.5$ ML), the first F atom prefers to add along the dangling bond of a silicon dimer, rather than bridge a Si-Si dimer bond. If an F atom approaches the surface at a significantly different angle than the dangling-bond direction, it is likely to encounter an attractive force and diffuse toward the dangling bond with no activation barrier.

B. Reaction of F atoms with the Si(100)-2×1 surface at 0.5 ML $<\Theta_F \le 1.0$ ML

After one Si-F bond is formed on each Si dimer, one dangling-bond orbital remains. Saturation of this unpaired electron by another atomic F is expected to be the most energetically favored reaction. Another possible pathway for an F atom would be formation of a SiF_2 group, requiring cleavage of the Si-Si dimer σ bond. Our calculations indicate that monofluorination (to form F-Si-Si-F) is preferred over difluorination (to form Si + SiF_2). We now discuss the details of these two possible reaction pathways.

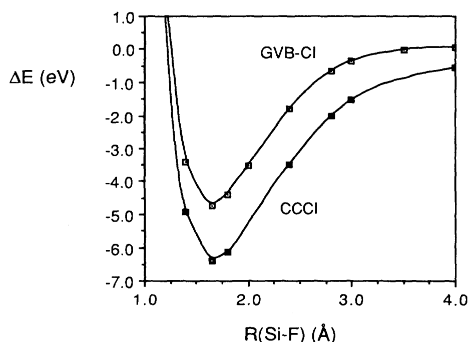

FIG. 5. Potential curves for a fluorine atom approaching a silicon dimer along the dangling-bond direction as a function of the Si-F distance [R(Si-F)], generated at the GVB-CI and CCCI levels for the GM-$Si_2\overline{H}_4F$ cluster.

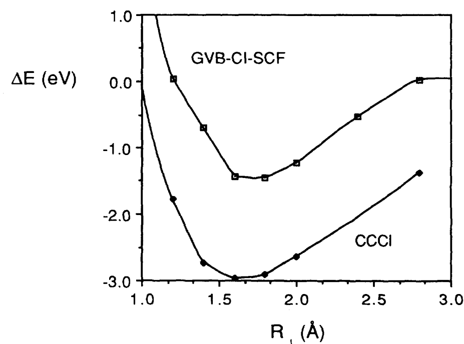

FIG. 6. Potential curves for a fluorine atom adsorbing onto a bridge site of a silicon dimer as a function of the perpendicular distance ($R_{\perp}$) between the fluorine atom and the Si(100)-2×1 surface, generated at the GVB-CI-SCF and CCCI levels for the GM-$Si_2\overline{H}_4F$ cluster.

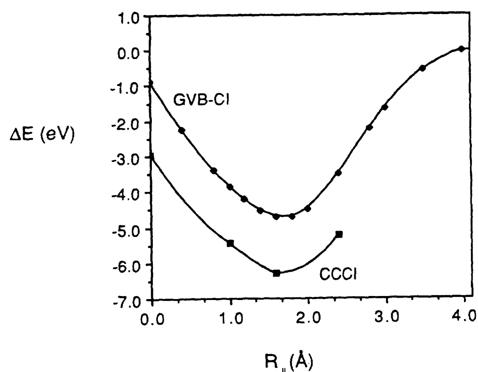

FIG. 7. Potential curves for fluorine atom diffusion from the twofold bridge-bonded position ($R_{\parallel}=0$ Å) to the onefold dangling-bond site of a silicon dimer ($R_{\parallel}=1.6$ Å), as a function of the parallel distance ($R_{\parallel}$) between the F atom and the original twofold bridge-bonded position. The vertical distance between the F atom and the surface was kept fixed at $R_{\perp,\text{eq}}=1.6$ Å. Both GVB-CI and CCCI levels for the GM-$Si_2\overline{H}_4F$ cluster are shown.

1. *Monofluorination*

In order to predict the equilibrium structure of an F-Si-Si-F species, the structure of the $Si_9\overline{H}_{12}F_2$ cluster was optimized at the GVB(3/6)-PP level, where the two Si-F bonds and the Si-Si dimer σ bond were correlated as GVB pairs. The optimized $Si_9\overline{H}_{12}F_2$ cluster is shown in Fig. 1(e), while the geometrical parameters of this cluster are given in Table VII. The equilibrium bond lengths of the Si-F and the Si-Si dimer are 1.643 and 2.435 Å, respectively, while the angle between the Si-F bond to surface normal is 23.1°, very close to the geometry of the first Si-F bond. In addition, the $Si_9\overline{H}_{12}F_2$ cluster exhibits symmetric and antisymmetric Si-F stretching frequencies at 612 and 919 cm^{-1}, respectively. The bending motions of F atoms are mixed with the other vibrational modes of the lattice in the low-frequency range of ~205–375 cm^{-1}. Again, these geometries and vibrational frequencies are close to those calculated or measured previously.[14,30]

The second Si-F bond is similar in character to that of the first Si-F bond. For instance, Mulliken population analysis of the optimized $Si_9\overline{H}_{12}F_2$ cluster reveals that 0.39e is transferred to the F atom directly from the Si atom to which it is bonded, while all subsurface Si atoms retain nearly the same charge distribution as the bare Si cluster and the optimized $Si_9\overline{H}_{12}F$ cluster (Table III). One-electron GVB contour plots of the three GVB bond pairs (the two Si-F σ bonds and the Si-Si dimer σ bond) for the optimized $Si_9\overline{H}_{12}F_2$ cluster are displayed in Fig. 8. Qualitatively, we see that the Si-F interaction is again extremely localized to the surface region.

The binding energy for the second Si-F bond of an F-Si-Si-F species calculated from both the larger ($Si_9\overline{H}_{12}F$ and $Si_9\overline{H}_{12}F_2$) and the smaller GM ($Si_2\overline{H}_4F$ and $Si_2\overline{H}_4F_2$) clusters are tabulated as a function of electron correlation in Tables IV and VIII, respectively. GVB-CI calculations on both clusters again show that the error incurred by replacing the larger $Si_9\overline{H}_{12}F_x$ clusters with the smaller GM-$Si_2\overline{H}_4F_x$ clusters is less than 0.1 eV. Our best prediction (CCCI) of the second Si-F bond strength calculated from the smaller GM $Si_2\overline{H}_4F$ and $Si_2\overline{H}_4F_2$ clusters is 6.1 eV, 0.3 eV smaller than the first Si-F bond.

Once the dangling bonds are saturated, the surface is covered with F-Si-Si-F species where the Si-Si dimer bonds remain intact ($\Theta_F=1.0$ ML, shown below).

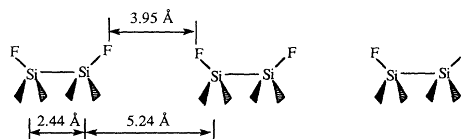

The nearest Si-Si distance between neighboring dimers in

TABLE VII. The important internal coordinates of the optimized $Si_9\overline{H}_{12}F_2$ cluster. Labels refer to Fig. 1(e).

Bond length (Å)		Bond angle (deg)	
R(F(1)-Si(1))		θ(F(1)-Si(1)-Si(2))	
=R(F(2)-Si(2))	1.643	=θ(F(2)-Si(2)-Si(1))	113.1
R(Si(1)-Si(2))	2.435	θ(F(1)-Si(1)-Si(3))	
R(Si(1)-Si(3))		=θ(F(1)-Si(1)-Si(5))	
=R(Si(1)-Si(5))		=θ(F(2)-Si(2)-Si(4))	
=R(Si(2)-Si(4))		=θ(F(2)-Si(2)-Si(6))	114.5
=R(Si(2)-Si(6))	2.348	θ(Si(3)-Si(1)-Si(5))	
R(Si(3)-Si(7))		=θ(Si(4)-Si(2)-Si(6))	104.4
=R(Si(5)-Si(8))		θ(Si(3)-Si(1)-Si(2))	
=R(Si(4)-Si(7))		=θ(Si(5)-Si(1)-Si(2))	
=R(Si(6)-Si(8))	2.362	=θ(Si(4)-Si(2)-Si(1))	
R(Si(7)-Si(9))		=θ(Si(6)-Si(2)-Si(1))	104.7
=R(Si(8)-Si(9))	2.352		
R(Si(3)-Si(4))			
=R(Si(5)-Si(6))	3.624		
R(Si(3)-Si(5))			
=R(Si(4)-Si(6))	3.608		
R(Si(7)-Si(8))	3.840		

adjacent rows is 5.24 Å, while the F-F nearest-neighbor distance is 3.95 Å in adjacent rows and 3.84 Å in the same dimer row. At this surface coverage, we find that no repulsion exists between fluorines bonded to neighboring dimers, either in the same row or adjacent rows.

2. *Difluorination*

Difluorination is modeled by the process shown below.

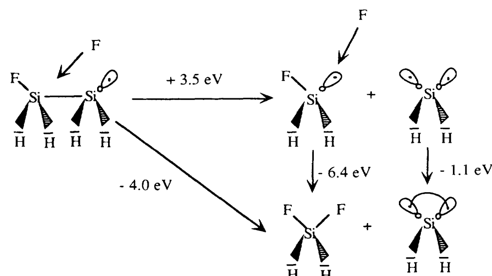

The $SiF_2\overline{H}_2$ cluster [shown in Fig. 1(g)] was fully optimized at the GVB (2/4)-PP level with two Si-F bonds treated as GVB pairs. This small cluster was chosen to model $SiF_{2(ad)}$. The geometrical parameters of this cluster are listed in Table IX. The equilibrium Si-F bond length in the SiF_2 species is 1.618 Å, which is close to that of the monofluorosilyl species. The angle between the Si-F bond and the surface normal for $SiF_{2(ad)}$ is predicted to be 54.3°, 30.8°closer to the silicon surface than for $SiF_{(ad)}$. The optimized $\overline{H}$-Si-$\overline{H}$ angle is 113.8°, which is only 4.4° larger than the ideal tetrahedral Si-Si-Si angle expected on the surface. Thus, the optimized $Si\overline{H}_2F_2$ cluster should be a reasonable first approximation to $SiF_{2(ad)}$. From Mulliken population analysis (listed in Table III), we find that each F atom in $SiF_{2(ad)}$ is less ionic (with $0.21e$ transferred to each F) than an F atom in an F-Si-Si-F species. However, the total positive charge on the Si atom in a difluorosilyl group is about double $(+0.41e)$ that of a monofluorosilyl group in the GM-$Si_2\overline{H}_4F_x$ cluster, suggesting that core-level shifts in the XPS spectra are indeed excellent ways of distinguishing $SiF_{(ad)}$ from $SiF_{2(ad)}$.[12,14–19]

The energetics of this process at our best level of calculation (CCCI) are displayed in the above picture. Table X lists the total energies of all clusters modeling this process. Forming a $SiF_{2(ad)}$ group from an F-Si-Si group requires initial cleavage of the Si-Si dimer bond in the F-Si-Si species at a cost of 3.5 eV, leading to a monofluorosilyl $SiF_{(ad)}$ species and a bare surface Si atom with two unpaired dangling bonds (if no electronic relaxation is allowed). Difluorination occurs when an incoming F atom attaches to the dangling bond of the $SiF_{(ad)}$ species to form a Si-F bond (downhill by 6.4 eV). Coupling the two dangling orbitals of the bare surface Si releases another 1.1 eV of energy. Thus, the effective Si-F bond strength of a $SiF_{2(ad)}$ species is predicted to be 4.0 eV, ~2.1 eV less exothermic than the monofluorination

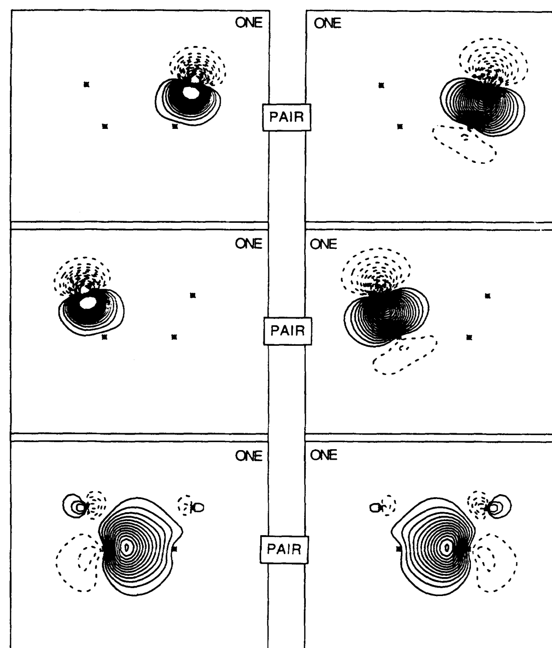

FIG. 8. Contour plots of one-electron GVB orbitals for the right Si-F σ-bond pair (top), the identical left Si-F σ-bond pair (middle), and the silicon dimer σ-bond pair (bottom) for the optimized $Si_9\overline{H}_{12}F_2(^1A_1)$ cluster.

TABLE VIII. The Si-F bond energy of an F-Si-Si-F species (D_e, in eV) obtained from calculations on the GM $Si_2\overline{H}_4F$ and $Si_2\overline{H}_4F_2$ clusters. The corresponding number of spatial configurations and spin eigenfunctions for each wave function are given beneath each total energy. The geometries of the GM $Si_2\overline{H}_4F$ and $Si_2\overline{H}_4F_2$ clusters were taken from the optimized $Si_9\overline{H}_{12}F$ and $Si_9\overline{H}_{12}F_2$ clusters (see text).

Calculation	Total energies (hartrees) $Si_2\overline{H}_4F_2$ $(^1A_1)$	$Si_2\overline{H}_4F$ $(^2A')$	D_e $(Si_2\overline{H}_4F\text{-}F)$
GVB(3/6)-PP	−778.684 09	−679.112 80	4.8
	(8/8)	(4/4)	
GVB-RCI(3/6)	−778.684 27	−679.112 89	4.8
	(27/37)	(9/17)	
GVB-CI(3/6)	−778.685 23	−679.113 43	4.8
	(141/175)	(19/35)	
GVB-RCI(3/6)*$(SD)_{Si-F}$	−778.691 34	−679.115 35	4.9
	(6997/12 631)	(228/424)	
CCCI(3/6)	−778.797 29	−679.178 31	6.1
	(15 433/34 939)	(1760/6872)	

TABLE IX. Optimized geometry for the $Si\bar{H}_2F_2$ cluster.

R(Si-F(1))=R(Si-F(2))	1.618 Å
R(Si-$\bar{H}$(1))=R(Si-$\bar{H}$(2))	1.422 Å
θ(F(1)-Si-$\bar{H}$(1))=θ(F(2)-Si-$\bar{H}$(2))	108.4°
θ(F(1)-Si-F(2))	108.6°
θ($\bar{H}$(1)-Si-$\bar{H}$(2))	113.8°

process, because of the cost to break the partially fluorinated Si dimer bond. Thus, for a perfect Si(100)-2×1 surface, monofluorination should occur before difluorination. However, difluorination may happen early in the etching process at defect sites on a real surface, since the silicon atoms at defect sites are expected to be highly unsaturated.

C. Fluorine adsorption on Si(100) for 1.0 ML $< \Theta_F \le 1.5$ ML

At $\Theta_F = 1.0$ ML on a perfect Si(100)-2×1 surface, the dangling bonds of all the dimers are saturated. Adding a third fluorine to this region of the surface now requires cleaving Si-Si bonds. We examined cleavage of the Si dimer bond to form a SiF_2 and a SiF species on the surface. The incipient Si-F bond is expected to be weaker than the first two Si-F bonds formed on the dimer because of the cost to break the Si-Si bond. As a first approximation, we ignored lattice relaxation and interactions between fluorine atoms attached to adjacent Si atoms. We used the following simple model to represent this reaction:

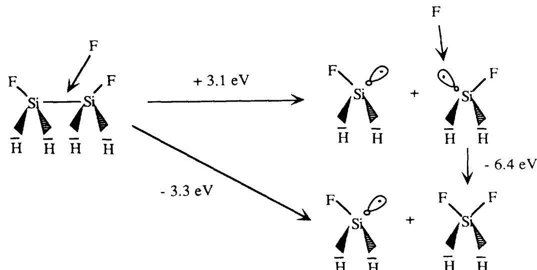

The energetics of this pathway obtained at the CCCI level are depicted in the above scheme, while the CCCI total energies for the above clusters are listed in Table X. We see that formation of $SiF_{2(ad)}$ and $SiF_{(ad)}$ from F-Si-Si-F groups is exothermic by 3.3 eV, since breaking F-Si-Si-F into two $SiF_{(ad)}$ species costs 3.1 eV, and the new Si-F bond formed releases 6.4 eV of energy.

As the fluorine coverage increases, the repulsion between neighboring fluorine atoms becomes significant. Thus, we constructed a more refined model that considers lateral interactions between the fluorosilyl groups. We investigated these lateral interactions for two surface configurations: (i) $\Theta_F = 1.25$ ML [a $p(4\times1)$ unit cell] and (ii) $\Theta_F = 1.5$ ML [a $p(2\times1)$ unit cell] shown in Figs. 9 and 10, respectively. We calculated the interaction energy in each repeat unit for surface structures (i) and (ii) by varying the distances between pairs of fluorosilyl groups [shown in Figs. 11(a)–11(e)]. Since the angles α and β are nearly identical ($\alpha = 35°$ and $\beta = 33°$), we assumed that (i) repulsion for the case in Fig. 11(a) is equal to the case in Fig. 11(b), where an F-Si-Si-F group approaches a SiF_2 or an FSi group; (ii) repulsion for the case in Fig. 11(d) is equal to the case in Fig. 11(e), where a SiF_2 group approaches another SiF_2 or an FSi group; and (iii) that R_1 is equal to R_3 in Fig. 9. To refine the model further, we also accounted for basis-set superposition errors (BSSE) (Ref. 45) for these nonbonded interactions in Figs. 11(a), 11(c), and 11(d) at the GVB-PP level. These BSSE are plotted as a function of the distance between two neighboring Si atoms in different fluorosilyl units [R(Si-Si)] in Figs. 12, 13, and 14, respectively. Taking into account the superposition errors, we plotted the lateral repulsion energies as a function of R(Si-Si) for the cases in Figs. 11(a), 11(c), and 11(d) in Figs. 15, 16, and 17, respectively. Crystallographic symmetry of the Si(100) surface constrains $R_1+R_2+R_3$ in Fig. 9 to be $4\times3.84-2.44=12.92$ Å, where 3.84 Å is the crystallographically imposed nearest-neighbor Si-Si distance on the unreconstructed Si(100) surface and 2.44 Å is the Si-Si dimer bond length of an F-Si-Si-F species obtained from the optimization of the $Si_9\bar{H}_{12}F_2$ cluster (see Table VII). Assuming $R_1 \sim R_3$, then we can solve for $R_2 \sim 12.92$ Å$-2R_1$, by searching for the minimum in lateral repulsions between fluorosilyl groups. We summed up the total repulsion energy in each repeat unit of the $p(4\times1)$ surface structure ($\Theta_F = 1.25$ ML, Fig. 9) and plotted them as a function of R_2 in Fig. 18. Similarly, in

TABLE X. Total energies (hartrees) at the CCCI level for all molecules in the cycles shown in Secs. III B 2 and III C.

Calculation[a]	$Si_2\bar{H}_4F_2$ ($^1A_1$)	$Si_2\bar{H}_4F$ ($^2A'$)	$Si\bar{H}_2F_2$ ($^1A_1$)	$Si\bar{H}_2F$ ($^2A'$)	$Si\bar{H}_2$ ($^3B_1$)	$Si\bar{H}_2$ ($^1A_1$)
CCCI	−778.862 06[b] (15 433/34 939)	−679.247 81[c] (2940/10 070)	−489.005 55[d] (3215/5098)	−389.374 85[e] (294/736)	−289.744 20[f] (17/33)	
GVB-RCI*(SD)$_{\text{dangling bond}}$					−289.742 53[g] (21/21)	−289.783 98[g] (34/34)

[a]Calculational details are given in Sec. II. The HF total energy for the F atom within the VDZP + DIF basis used here is −99.395 61 hartrees. 1 hartree equals 627.5096 kcal/mol equals 27.211 62 eV = 219 474.8 cm^{-1}. The corresponding number of spatial configurations and spin eigenfunctions for each wave function are given beneath each total energy.
[b]CCCI = GVB-RCI(3/6)*[(SD)$_{Si\text{-}Si}$+S_{val}] for breaking the Si-Si bond in the cycle shown in Sec. III C.
[c]CCCI = GVB-RCI(2/4)*[(SD)$_{Si\text{-}Si}$+S_{val}] for breaking the Si-Si bond in the cycle shown in Sec. III B 2.
[d]CCCI = GVB-RCI(2/4)*[(SD)$_{Si\text{-}F}$+S_{val}] for breaking the Si-F bond in the cycles shown in Secs. III B 2 and III C.
[e]CCCI = GVB-RCI(1/2)*S_{val} for the $Si\bar{H}_2F$ fragment in the cycles shown in Secs. III B 2 and III C.
[f]CCCI = HF*S_{val} for the $Si\bar{H}_2$ ($^3B_1$) fragment in the cycle shown in Sec. III B 2.
[g]CI for calculating the singlet-triplet splitting in $Si\bar{H}_2$, shown in the cycle in Sec. III B 2. See Ref. 33 for calculational details.

$R_1 = 4.36$ Å $R_2 = 4.20$ Å $R_3 = 4.36$ Å

p (4 x 1) $\Theta_F = 1.25$ ML

FIG. 9. The $p(4\times1)$ equilibrium surface structure at $\Theta_F = 1.25$ ML.

$R_4 = 3.10$ Å $R_5 = 4.58$ Å

p (2 x 1) $\Theta_F = 1.5$ ML

FIG. 10. The $p(2\times1)$ equilibrium surface structure at $\Theta_F = 1.5$ ML.

(a) (b) (c) (d) (e)

FIG. 11. Schematic pictures of the five cases considered in calculations of the lateral repulsion between pairs of fluorosilyl species.

ΔE (eV) R(Si-Si) (Å)

FIG. 12. Basis-set superposition error (BSSE) calculated at the GVB-PP level for the cases in Figs. 11(a) and 11(b), where an F-Si-Si-F approaches a SiF_2 or an FSi species. The BSSE is plotted as a function of distance between the two neighboring Si atoms in the two fluorosilyl species (R_{Si-Si}).

ΔE (eV) R(Si-Si) (Å)

FIG. 13. BSSE calculated at the GVB-PP level for the case in Fig. 11(c), where an SiF_2 species approaches a SiF species, as a function of R_{Si-Si}.

ΔE(eV) R(Si-Si) (Å)

FIG. 14. BSSE calculated at the GVB-PP level for the cases in Figs. 11(d) and 11(e), where a SiF_2 species approaches another SiF_2 or an FSi species, as a function of R_{Si-Si}.

ΔE (eV) R(Si-Si) (Å)

FIG. 15. Potential curve calculated at the GVB-PP level (accounting for BSSE) for the cases in Figs. 11(a) and 11(b), where an F-Si-Si-F approaches a SiF_2 or an FSi species, as a function of R_{Si-Si}.

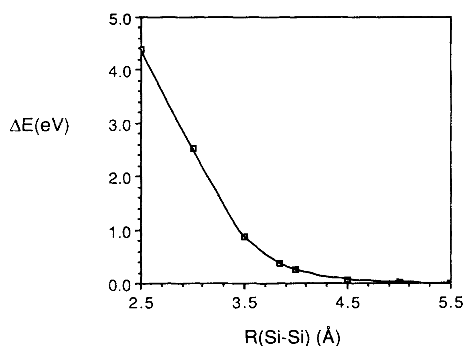

FIG. 16. Potential curve calculated at the GVB-PP level (accounting for BSSE) for the case in Fig. 11(c), where a SiF_2 species approaches a SiF species, as a function of R_{Si-Si}.

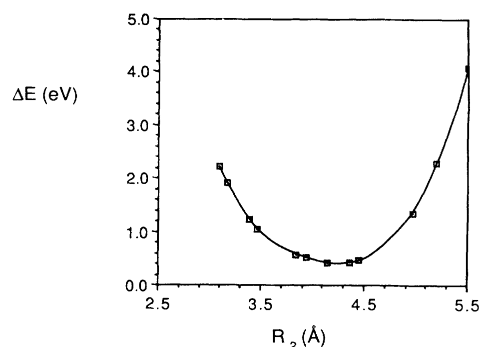

FIG. 18. Total repulsion energy in a unit cell of the $p(4\times1)$ surface structure ($\Theta_F=1.25$ ML, Fig. 9) generated at the GVB-PP level.

the $p(2\times1)$ surface structure ($\Theta_F=1.5$ ML, Fig. 10), we have $R_4+R_5=2\times3.84$ Å, or $R_5=7.68$ Å$-R_4$. The total repulsion energy in each $p(2\times1)$ unit is displayed as a function of R_4 in Fig. 19. The equilibrium geometries of the $p(4\times1)$ and the $p(2\times1)$ structures are found to be $R_1=R_3=4.36$ Å, $R_2=4.20$ Å, $R_4=3.10$ Å, and $R_5=4.58$ Å (shown in Figs. 9 and 10), while the lateral repulsions for both structures at equilibrium are 0.4 eV/[$p(4\times1)$ unit cell] and 3.1 eV/[$p(2\times1)$ unit cell], respectively.

Now, considering both lateral repulsions (and basis-set superposition errors) and bond breaking and forming, we predict that the formation of the $p(4\times1)$ structure ($\Theta_F=1.25$ ML) is downhill by $3.3-0.4=2.9$ eV from $\Theta_F=1.0$ ML. Addition of another F to this $p(4\times1)$ structure ($\Theta_F=1.25$ ML) to form the $p(2\times1)$ structure ($\Theta_F=1.5$ ML) is found to be endothermic by 2.5 eV, because of 3.1 eV/ [$p(2\times1)$ unit cell] repulsions for a surface with half SiF radicals and half SiF_2 groups at $\Theta_F=1.5$ ML. (The differential repulsion between $\Theta_F=1.5$ and 1.25 ML is $6.2-0.4=5.8$ eV/[$p(4\times1)$ unit cell], and the energy gained is only 3.3 eV from the newly formed Si-F bond, as in the $1.0\rightarrow1.25$ ML case.) Thus, at low exposures or with a dilute beam of F atoms, the $p(4\times1)$ structure involving a SiF_2, a SiF, and an F-Si-Si-F dimer may be a stable intermediate phase. However, if two F atoms attack neighboring F-Si-Si-F dimers simultaneously at $\Theta_F=1.0$ ML, it is favorable by 0.4 eV to form alternating SiF and SiF_2 groups on the surface.

This mechanism may be partially responsible for the different coverages reached upon initial adsorption of XeF_2 versus F_2.[15,19] Photoemission data[15] suggest that exposure of Si(100) to XeF_2 leads to an initial adsorption phase with 70% SiF and 23% SiF_2, which corresponds closely to the 1.25 ML structure we have proposed, shown in Fig. 9 (75% SiF and 25% SiF_2). Since our energetics suggest it may be possible to be trapped in this phase if two F atoms are not delivered to adjacent Si dimers simultaneously, it may be that XeF_2 decomposes via ejection of the last F atom with enough kinetic energy such that it does not adsorb right next to the first F atom. This is plausible, since XeF is unstable. By contrast, F_2 beams exhibit fast adsorption kinetics up to 1.5 ML, after which the rate drops off precipitously.[19] It may be that F_2 dissociatively adsorbs with both F atoms delivered to neighboring dimers, since our calculations suggest this is

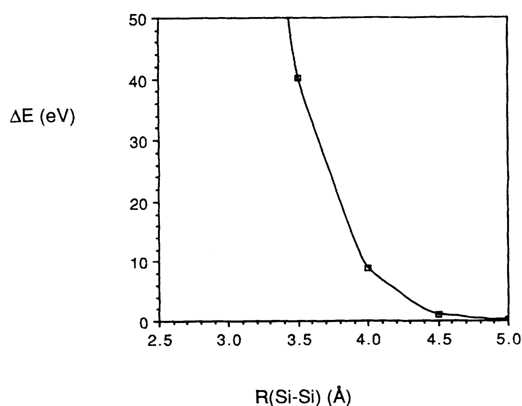

FIG. 17. Potential curve calculated at the GVB-PP level (accounting for BSSE) for the cases in Figs. 11(d) and 11(e), where a SiF_2 species approaches another SiF_2 or an FSi species, as a function of R_{Si-Si}.

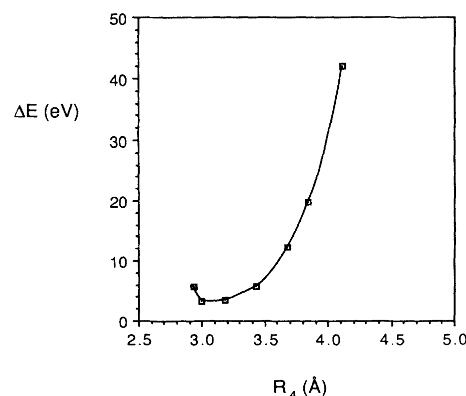

FIG. 19. Total repulsion energy in a unit cell of the $p(2\times1)$ surface structure ($\Theta_F=1.5$ ML, Fig. 10) generated at the GVB-PP level.

the only way to reach $\Theta_F = 1.5$ ML.

An ordered $p(3\times1)$ overlayer on Si(100) has been reported by Chabal and Raghavachari[53] for hydrogen adsorption, which was also observed later by Boland[54] using scanning tunneling microscopy (STM). This $p(3\times1)$ phase was suggested to involve repeated alternation of monohydride and dihydride units.[54] Although such a $p(3\times1)$ phase ($\Theta_F = 1.33$ ML) has never been reported for F on Si(100), for completeness we calculated the lateral interactions between the analogous adspecies, in order to compare their stabilities relative to $\Theta_F = 1.25$ and 1.5 ML. The ideal $p(3\times1)$ structure is shown below:

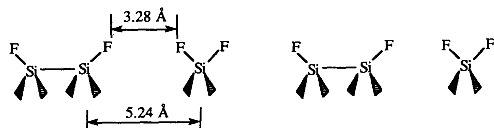

The lateral repulsions between neighboring F-Si-Si-F and SiF_2 groups are found to be negligible (see Fig. 15) because the distance between adjacent fluorines in neighboring F-Si-Si-F and SiF_2 groups is 3.28 Å, which corresponds to R(Si-Si) = 5.24 Å. Thus, in principle, we expect this phase to be accessible. However, formation of this $p(3\times1)$ phase requires not only Si dimer bond breaking and Si-F bond formation, but it also must involve some complicated surface rearrangement to convert from the $p(2\times1)$ to $p(3\times1)$ phase, which we leave for future work.

D. Fluorine adsorption on Si(100) for 1.5 ML $< \Theta_F \leq 2.0$ ML

After the third fluorine breaks the Si dimer bond to form SiF_2 and SiF groups, a dangling-bond orbital remains on the SiF group. The saturation of this dangling-bond orbital is modeled by the following process:

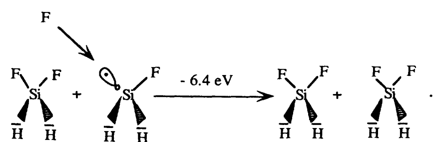

The CCCI prediction of the isolated Si-F bond energy is 6.4 eV (the CCCI total energies for the optimized $Si\bar{H}_2F$ and $Si\bar{H}_2F_2$ clusters are listed in Table X). However, the surface would now be saturated by SiF_2 species with only 3.84 Å between each Si, the same as that on the $p(1\times1)$ unreconstructed Si(100) surface, as shown below.

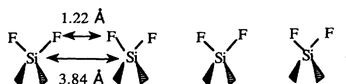

At this distance, assuming the SiF_2 groups retain tetrahedral coordination, the fluorine atoms are closer to each other ($R_{F\text{-}F} = 1.22$ Å) than in the F_2 molecule ($R_{F\text{-}F} = 1.41$ Å). Therefore, we expect that repulsions between F atoms will dictate the surface structure at this coverage. Figure 17 shows the GVB-PP potential curve (including the counterpoise correction for superposition error) for two SiF_2 groups approaching each other with all four fluorines in the same plane [shown in Fig. 11(e)]. At the crystallographically imposed Si-Si distance of 3.84 Å, the repulsion between two neighboring SiF_2 groups is ~17 eV, much larger than the Si-F bond energy. Thus, we predict a large barrier for addition of more F atoms beyond $\Theta_F = 1.5$ ML, consistent with the decrease in the rate of adsorption of F atoms in this coverage range.[19]

It is possible that the SiF_2 groups will attempt to move away from one another by relaxing the constraint of having the Si atoms remain tetrahedral. Therefore, we studied the effect of rotating a SiF_2 species by twisting both F atoms on a SiF_2 group simultaneously (see below).

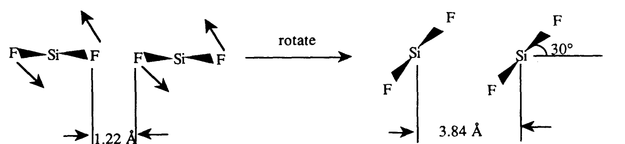

This indeed reduced the repulsion between two neighboring SiF_2 groups, but at the same time it weakens the Si-Si bonds. A crude estimate of the strain energy caused by twisting was calculated at the GVB-PP level using the optimized $Si\bar{H}_2F_2$ cluster and is plotted as a function of the twisting angle in Fig. 20. The repulsion energy generated at the GVB-PP level between two concertedly twisted SiF_2 groups is displayed in Fig. 21 as a function of the twist angle. We find that concerted twisting of the SiF_2 groups minimizes this repulsion (down to 1.8 eV) at a 30° twist, but this introduces considerable subsurface strain (~1.3 eV). Our strain estimate may be a lower bound, since our model contains spherical $\bar{H}$'s instead of the directional sp^3-like orbitals on true subsurface Si atoms. This directionality should cause the strain to be even greater than 1.3 eV. However, inclusion of higher levels of electron correlation may decrease the strain energy. Therefore, these two effects may cancel. Thus, although SiF_2 is known to be an extremely stable species in the gas phase, it is predicted to be much less favorable than SiF on the surface because of unfavorable lateral interactions. LEED and photoemission data for low exposures of XeF_2 on Si(100)-2×1 also support these predictions.[14,15] Thus, further fluorination and etching may have to proceed sequentially, whereby patches of Si are etched away be-

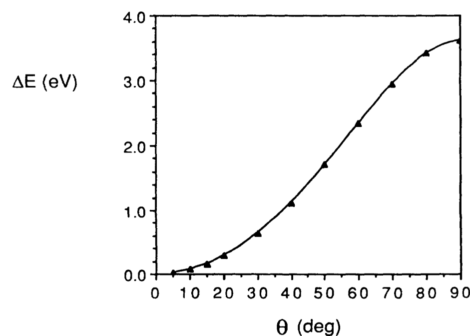

FIG. 20. Strain energy as a function of twisting angle θ, calculated at the GVB-PP level, for twisting two Si-F bonds simultaneously in the optimized $Si\bar{H}_2F_2$ cluster.

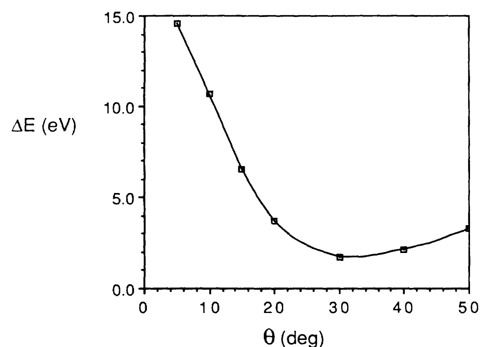

FIG. 21. Total repulsion energy as a function of twisting angle θ between the two twisting SiF_2 groups, generated at the GVB-PP level.

fore others, due to the propensity of SiF_2 to etch more quickly because of its instability. Indeed, recent STM work by Boland[55] examining H-atom etching of Si(100) confirms this idea. Even in this system where the H-H repulsions are much smaller than the F-F repulsions,[56] adjacent SiH_2's are preferentially etched.

IV. SUMMARY

We have presented first-principles quantum-mechanical calculations examining the reaction of atomic fluorine with the Si(100)-2×1 surface. We find that fluorine atoms first attack dangling bonds of dimers and saturate the surface with $SiF_{(ad)}$ species at lower fluorine coverages (≤ 1.0 ML). At this stage, the reaction is very exothermic, with heats of reaction ~ 6.3 eV/F. Formation of $SiF_{2(ad)}$ should occur only after all dangling bonds on the Si dimers are saturated. However, the repulsion between adjacent F atoms naturally increases as the fluorine coverage increases, making difluorination more difficult at higher coverages (1.5 ML $\leq \Theta \leq 2.0$ ML). We have suggested that this may have implications for fluorine adsorption kinetics as a function of coverage and precursor (e.g., XeF_2 or F_2). A uniform SiF_2 surface configuration ($\Theta_F = 2.0$ ML) will not form, due to huge activation barriers resulting from fluorine repulsions. Thus, unless the lattice is strained via SiF_2 twisting, F-F repulsions inhibit formation of a SiF_2-covered surface. However, such lattice strain may in fact facilitate the etching process, via weakening the Si-Si bonds.

ACKNOWLEDGMENTS

This work was supported by the Air Force Office of Scientific Research (Grant No. AFOSR-89-0108). E.A.C. also acknowledges support of the National Science Foundation and the Camille and Henry Dreyfus Foundation. C.J.W. is grateful for partial support from Products Research Corporation.

[1]J. L. Mauer, J. S. Logan, L. B. Zielinski, and G. C. Schwartz, J. Vac. Sci. Technol. **15**, 1734 (1978).
[2]J. W. Coburn and H. F. Winters, J. Vac. Sci. Technol. **16**, 391 (1979).
[3]J. W. Coburn, Plasma Chem. Plasma Proc. **2**, 1 (1982).
[4]J. W. Coburn and H. F. Winters, Annu. Rev. Mater. Sci. **13**, 91 (1983).
[5]H. F. Winters, J. W. Coburn, and T. J. Chuang, J. Vac. Sci. Technol. B **1**, 469 (1983).
[6]Y. Y. Tu, T. J. Chuang, and H. F. Winters, Phys. Rev. B **23**, 823 (1981).
[7]D. L. Flamm, V. M. Donnelly, and J. A. Mucha, J. Appl. Phys. **52**, 3633 (1981).
[8]J. A. Mucha, V. M. Donnelly, D. L. Flamm, and L. M. Webb, J. Phys. Chem. **85**, 3529 (1981).
[9]M. J. Vasile and F. A. Stevie, J. Appl. Phys. **53**, 3799 (1982).
[10]H. F. Winters and F. A. Houle, J. Appl. Phys. **54**, 1218 (1983).
[11]D. E. Ibbotson, D. L. Flamm, J. A. Mucha, and V. M. Donnelly, Appl. Phys. Lett. **44**, 1129 (1984).
[12]C. D. Stinespring and A. Freedman, Appl. Phys. Lett. **48**, 718 (1986).
[13]F. A. Houle, J. Appl. Phys. **60**, 3018 (1986).
[14]N. D. Shinn, J. F. Morar, and F. R. McFeely, J. Vac. Sci. Technol. A **2**, 1593 (1984).
[15]F. R. McFeely, J. F. Morar, N. D. Shinn, G. Landgren, and F. J. Himpsel, Phys. Rev. B **30**, 764 (1984).
[16]F. R. McFeely, J. F. Morar, and F. J. Himpsel, Surf. Sci. **165**, 277 (1986).
[17]F. R. McFeely, B. D. Silverman, J. A. Yarmoff, and U. O. Karlsson, in *Proceedings of the Eighth International Symposium on Plasma Chemistry,* edited by K. Akashi and A. Kinbara (International Union of Pure and Applied Chemistry, Tokyo, 1987), p. 927.
[18]J. R. Engstrom, M. M. Nelson, and T. Engel, Phys. Rev. B **37**, 6563 (1988).
[19]J. R. Engstrom, M. M. Nelson, and T. Engel, Surf. Sci. **215**, 437 (1989).
[20]M. J. Bozack, M. J. Dresser, W. J. Choyke, P. A. Taylor, and J. T. Yates, Jr., Surf. Sci. **184**, L332 (1987).
[21]A. L. Johnson, M. M. Walczak, and T. E. Madey, Langmuir **4**, 277 (1988).
[22]M. Seel and P. S. Bagus, Phys. Rev. B **28**, 2023 (1983).
[23]P. S. Bagus, in *Plasma Synthesis and Etching of Electronic Materials,* edited by R. P. H. Chang and B. Abeles, MRS Symposia Proceedings No. 38 (Materials Research Society, Pittsburgh, 1985), p. 179.
[24]F. Illas, J. Rubio, and J. M. Ricart, Phys. Rev. B **31**, 8068 (1985).
[25]S. M. Mohapatra, B. N. Dev, K. C. Mishra, N. Sahoo, W. M. Gibson, and T. P. Das, Phys. Rev. B **38**, 12 556 (1988).
[26]B. J. Garrison and W. A. Goddard III, Phys. Rev. B **36**, 9805 (1987).
[27]P. J. van den Hoek, W. Ravenek, and E. J. Baerends, Phys. Rev. B **38**, 12 508 (1988).
[28]C. G. van de Walle, Y. Bar-Yam, F. R. McFeely, and S. T. Pantelides, J. Vac. Sci. Technol. A **6**, 1973 (1988).
[29]C. G. van de Walle, F. R. McFeely, and S. T. Pantelides, Phys. Rev. Lett. **61**, 1867 (1988).
[30]B. I. Craig and P. V. Smith, Surf. Sci. **239**, 36 (1990).
[31]F.W. Bobrowicz and W. A. Goddard III, *Methods of Electronic Structure Theory* (Plenum, New York, 1977), Vol. 3.
[32]E. A. Carter and W. A. Goddard III, J. Chem. Phys. **88**, 3132

(1988).
[33]E. A. Carter and W. A. Goddard III, J. Chem. Phys. **88**, 1752 (1988).
[34]A preliminary account of this work has appeared [C. J. Wu and E. A. Carter, J. Am. Chem. Soc. **113**, 9061 (1991)].
[35]D. Haneman, Rep. Prog. Phys. **50**, 1045 (1987).
[36]C. J. Wu and E. A. Carter, Chem. Phys. Lett. **185**, 172 (1991).
[37]A. K. Rappé, T. A. Smedley, and W. A. Goddard III, J. Phys. Chem. **85**, 1662 (1981).
[38]A. Redondo, W. A. Goddard III, C. A. Swarts, and T. C. McGill, J. Vac. Sci. Technol. **19**, 498 (1981).
[39]T. H. Dunning, Jr., J. Chem. Phys. **53**, 2823 (1970).
[40]S. Huzinaga, J. Chem. Phys. **42**, 1293 (1965).
[41]M. Dupuis and H. F. King, J. Chem. Phys. **68**, 3998 (1978).
[42]H. B. Schlegel, J. Comput. Chem. **3**, 214 (1982).
[43]C. J. Wu and E. A. Carter, J. Am. Chem. Soc. **112**, 5893 (1990).
[44]C. J. Wu and E. A. Carter, J. Phys. Chem. **95**, 8352 (1991).
[45]S. F. Boys and F. Bernardi, Mol. Phys. **19**, 553 (1970).
[46]A. Redondo and W. A. Goddard III, J. Vac. Sci. Technol. **21**, 344 (1982).
[47]C. Kittel, *Introduction to Solid State Physics*, 6th ed. (Wiley, New York, 1986).
[48]M. D. Harmony, V. W. Laurie, R. L. Kuczkowski, R. H. Schwendeman, D. A. Ramsay, F. J. Lovas, W. J. Lafferty, and A. G. Maki, J. Phys. Chem. Ref. Data **3**, 619 (1979).
[49]R. Walsh, Acc. Chem. Res. **14**, 246 (1981).
[50]R. Walsh, J. Chem. Soc. Faraday Trans. 1 **79**, 2233 (1983).
[51]T. A. Schoolcraft and B. J. Garrison, J. Vac. Sci. Technol. A **8**, 3496 (1990).
[52]P. C. Weakliem, C. J. Wu, and E. A. Carter (unpublished).
[53]Y. J. Chabal and K. Raghavachari, Phys. Rev. Lett. **54**, 1055 (1985).
[54]J. J. Boland, Phys. Rev. Lett. **65**, 3325 (1990).
[55]J. J. Boland (unpublished).
[56]C. J. Wu and E. A. Carter (unpublished).

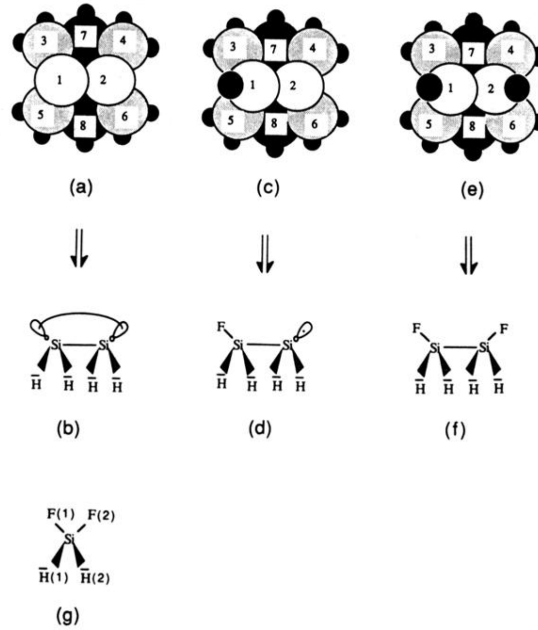

FIG. 1. Schematic pictures of silicon clusters used in calculations for modeling (i) the bare Si(100)-2×1 surface by (a) the fully optimized $Si_9\overline{H}_{12}$ cluster and (b) the GM-$Si_2\overline{H}_4$ cluster; (ii) a half-fluorinated silicon dimer (Si-Si-F) by (c) the fully optimized $Si_9\overline{H}_{12}F$ cluster and (d) the GM-$Si_2\overline{H}_4F$ cluster; (iii) a fully fluorinated silicon dimer (F-Si-Si-F) by (e) the fully optimized $Si_9\overline{H}_{12}F_2$ cluster and (f) the GM-$Si_2\overline{H}_4F_2$ cluster; and (iv) a difluorosilyl species (SiF_2) by (g) the fully optimized $Si_2\overline{H}_2F_2$ cluster. Si atoms in the $Si_9\overline{H}_{12}$ clusters are numbered from the surface layer downward. Small black circles represent $\overline{H}$ atoms. The fourth-layer Si atom is not shown. Medium-sized gray circles represent F atoms.